Photochemical & Photobiological Sciences

PAPER

Cite this: *Photochem. Photobiol. Sci.*, 2014, **13**, 1781

Temperature and oxygen-concentration dependence of singlet oxygen production by RuPhen as induced by quasi-continuous excitation

Jaroslav Varchola,[a] Veronika Huntosova,[b] Daniel Jancura,[a,b] Georges Wagnières,[c] Pavol Miskovsky[a,b] and Gregor Bánó*[a,b]

Assessment of partial pressure of oxygen (pO_2) by luminescence lifetime measurements of ruthenium coordination complexes has been studied intensively during the last few decades. RuPhen (dichlorotris-(1,10-phenanthroline) ruthenium(II) hydrate) is a water soluble molecule that has been tested previously for *in vivo* pO_2 detection. In this work we intended to shed light on the production of singlet oxygen by RuPhen. The quantum yield of singlet oxygen production by RuPhen dissolved in 0.9% aqueous NaCl solution (pH = 6) was measured at physiological temperatures (285–310 K) and various concentrations of molecular oxygen. In order to minimize the bleaching of RuPhen, the samples were excited with low power (<2 mW) laser pulses (20 μs long), created by pulsing a cw laser beam with an acousto-optical modulator. We show that, whereas the RuPhen phosphorescence lifetime decreases rapidly with an increase of temperature (keeping the oxygenation level constant), the quantum yield of singlet oxygen production by RuPhen is almost identical in the temperature range of 285–310 K. For air-saturated conditions at 310 K the measured quantum yield is about 0.25. The depopulation rate constants of the RuPhen ^{3}MLCT (metal-to-ligand charge-transfer) state are determined in the absence and in the presence of oxygen. We determined that the excitation energy for the RuPhen ^{3}MLCT→d–d transition is 49 kJ mol^{-1} in the 0.9% NaCl solution (pH = 6).

Received 6th June 2014,
Accepted 2nd October 2014

DOI: 10.1039/c4pp00202d

www.rsc.org/pps

Introduction

Photodynamic therapy (PDT) is one modality currently used for treating cancerous or non-cancerous diseases in different organs of the human body.[1–3] The ordinary PDT action is based on the interaction of light-activated drugs with the ground state (triplet, $O_2(^3\Sigma_g^-)$) molecular oxygen, resulting in the production of reactive oxygen species (in most cases singlet oxygen in the $O_2(^1\Delta_g)$ state). Thus, appropriate oxygenation of the treated area is of great importance for achieving high therapeutic efficiency of PDT. Monitoring the tissue oxygenation before, during and after the treatment is of interest to understand the mechanisms behind PDT and for optimizing the therapy procedures.[4–7] In addition, measuring the partial pressure of oxygen (pO_2) also provides valuable information on tissue metabolism.[8,9]

Oxygen concentration can be assessed, among other methods, by detecting luminescence characteristics of oxygen sensitive molecular probes.[10] In general, time-resolved or intensity-based luminescence techniques can be applied.[11,12] The very first molecular probes used for pO_2 detection by time-resolved phosphorescence measurements were metallo-porphyrins, oxygen-sensitive molecules with phosphorescence lifetimes of hundreds of microseconds.[10,13,14] The main limitation of using metallo-porphyrins for *in vivo* pO_2 detection is their high photo-toxicity induced by singlet oxygen production.[6,10,15] In this context, polypyridyl coordination complexes represent an attractive alternative with advantageous optical properties, and good chemical and photostability.[16,17] These complexes possess a relatively long-lived triplet ^{3}MLCT (metal-to-ligand charge transfer) state with strong phosphorescence emission in the visible spectral region. Effective quenching of the ^{3}MLCT state by molecular oxygen makes polypyridyl coordination complexes suitable for pO_2 measurements.[18]

RuPhen ($[Ru(Phen)_3]^{2+}$, dichlorotris(1,10-phenanthroline) ruthenium(II) hydrate) is a water-soluble member of the polypyridyl coordination complex family with a broad absorption band between 350 and 500 nm.[19,20] The phosphorescence

[a]*Department of Biophysics, Faculty of Science, P. J. Šafárik University, Jesenná 5., Košice 041 54, Slovak Republic. E-mail: gregor.bano@upjs.sk*
[b]*Center for Interdisciplinary Biosciences, Faculty of Science, P. J. Šafárik University, Jesenná 5., Košice 041 54, Slovak Republic*
[c]*ISIC-LCOM, Swiss Federal Institute of Technology (EPFL), Batiment CH, Station 6, CH-1015 Lausanne, Switzerland*

emission from the RuPhen ^{3}MLCT state (centered at 600 nm) was reported to be sensitive to local oxygen concentration.[21,22] From a clinical point of view, low dark toxicity and a relatively high clearance rate make RuPhen attractive for *in vivo* time-resolved pO_2 detection.[23–26] There are a few publications reporting on a weak photo-cytotoxicity of RuPhen.[27,28] These observations are in agreement with our preliminary results obtained *in vivo* with RuPhen applied to the chorioallantoic membrane (CAM) system.[29] By contrast, photodamage induced *in vitro* by RuPhen localized in the extracellular space has been reported.[30] Indeed, photo-excited RuPhen is known to produce singlet oxygen.[31,32] Moreover, many ruthenium polypyridyl complexes show antitumor activities related to DNA binding and photocleavage. The mechanism of these activities is partially connected to singlet oxygen production, but electron transfer processes and superoxide anion radical production may also play an important role here.[33–36]

Detailed studies on RuPhen ^{3}MLCT state depopulation and singlet oxygen production in deuterated methanol and deuterated water solutions have been published recently.[31,32] To the best of our knowledge, however, there are no data available in the literature for the quantum yield of singlet oxygen production by the highly environment sensitive RuPhen dissolved in water.

Singlet oxygen $O_2(^1\Delta_g)$ can be detected through its phosphorescence around 1270 nm.[37,38] Previous RuPhen-related singlet oxygen measurements were carried out by two different experimental approaches. In the first case, 355 nm laser pulses (third harmonic of a Q-switched Nd:YAG laser) were used for RuPhen photo-excitation, and the time-resolved luminescence of singlet oxygen was detected with a germanium photodiode.[39] When working with low repetition rate and short pulse (high peak power) lasers, one usually faces serious problems due to the photo-bleaching of the sample. An extrapolation of the measured singlet oxygen emission intensity slopes to zero excitation pulse energies was used by Schmidt and co-authors to correct the bleaching effects.[32,40] In the second case, excitation from a Xe/Hg lamp combined with a monochromator was used to induce singlet oxygen production by RuPhen.[31] Using this second approach, data evaluation relied on the steady-state phosphorescence intensity values.

In this work we applied a modified illumination strategy for time-resolved singlet oxygen measurements, where bleaching was circumvented by the use of low power laser excitation. Studied specimens were illuminated in a quasi-continuous mode: long (20 μs) laser pulses were applied to reach steady-state emission intensities and excited molecule concentrations in the sample. Once the laser was switched off, phosphorescence decays of both RuPhen and $O_2(^1\Delta_g)$ were detected. The residual phosphorescence emission from RuPhen at 1270 nm was readily distinguished from the $O_2(^1\Delta_g)$ signal based on the different decay times.

Long-pulse laser excitation was applied previously by Lee and co-authors to induce singlet oxygen production in a series of PDT-related measurements *in vitro*[41] and *in vivo*.[42] As the length of the excitation pulses was limited to less than 10 μs, steady-state emission intensities were typically not reached in these studies. The evolution of singlet oxygen concentration was simulated by the numerical solution of the corresponding kinetic model.[41,42] By contrast, in the present work the length of the excitation laser pulses was set to be longer (20 μs). In this quasi-continuous excitation mode the highest possible (steady-state) luminescence intensities were reached (for a given laser power) at the end of laser pulses. Moreover, the kinetic model describing excited state populations of RuPhen and molecular oxygen after switching the laser off could be solved analytically, facilitating thus the data evaluation procedure (see the Data analysis section below).

Our primary goal in this work was to quantify singlet oxygen production by photoexcited RuPhen in 0.9% isotonic aqueous NaCl solution (used in biological and clinical applications), covering the physiologically relevant temperatures and molecular oxygen concentrations. Moreover, temperature dependent rate constants for depopulation processes of the RuPhen ^{3}MLCT state were determined as a function of oxygen concentration. The possible consequences of singlet oxygen production by RuPhen for its utilization as *in vivo* pO_2 sensor are also discussed.

Experimental

Materials

RuPhen (dichlorotris(1,10-phenanthroline) ruthenium(II) hydrate) was purchased from Sigma-Aldrich and dissolved in 0.9% isotonic aqueous NaCl solution (pH = 6, Braun). Rose Bengal (Sigma-Aldrich) dissolved in water was used as a reference sample to calibrate the experimental apparatus for quantitative singlet oxygen measurements.

Experimental setup and procedures

The diagram of the experimental setup is shown in Fig. 1a. CW lasers operating at wavelengths of 476 nm (Coherent 90C FreD) and 532 nm (Cobolt Samba) were used for RuPhen and Rose Bengal excitation, respectively. The laser beams passed through an acousto-optical modulator (AOM, Isomet 1205C)

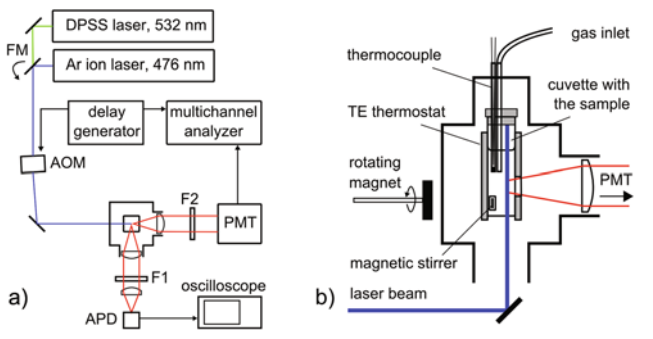

Fig. 1 (a) Diagram of the optical setup and the sample cell (top view). AOM – acousto-optic modulator, APD – avalanche photo-diode, F_1: >500 nm long-pass filter, F_2: 1250–1350 nm band-pass filter, FM – flipping mirror. (b) Side-view of the sample cell.

operated in switching (ON/OFF) mode. The AOM was driven by electrical pulses from a delay generator. The repetition rate of 20 μs laser pulses was set to 2 kHz. The laser beam diameter was 2 mm at the AOM, which limited the switching time of the AOM to approx. 400 ns.

2 ml of the sample solution was poured into a quartz cuvette (10 × 10 × 40 mm), which was placed in a temperature regulated sample cell (Fig. 1b). The absorbance of the RuPhen and Rose Bengal solutions were set to be equal (0.052) at the excitation wavelengths of 476 and 532 nm, as measured with a Shimadzu UV-2401PC UV-VIS spectrophotometer. The corresponding concentration of RuPhen (about 10 μM) was low enough to avoid self-absorption of the phosphorescence inside the cuvette.[27] The sample temperature was monitored directly in the solution by a thermocouple enclosed in a glass capillary. The cell was either cooled or heated thermoelectrically using an automated regulation scheme.

Two gas-flow controllers were applied to mix pure N_2 and O_2 gases to a final O_2 concentration of 5–40% in the gas phase. 25 standard cubic centimeters per minute (sccm) of the gas mixture were introduced into the cuvette through a glass capillary for 1 hour before the measurements, thus enabling the system to reach steady-state oxygen concentration. The mixed gas was continuously flowing through the cuvette during the measurements. The dissolved-oxygen concentration in the air-saturated 0.9% NaCl solution was evaluated by interpolating the tabulated data of Benson and Krause.[43] A magnetic stirrer was applied to stir the solutions during the measurements.

The laser beam entered the cuvette from the bottom (Fig. 1b). The average laser power at the sample was 0.7 mW for 476 nm and 1.7 mW for 532 nm. Emission from the sample was detected at 90° in two channels. The visible phosphorescence signal from RuPhen passed through a long-pass filter (>500 nm), and was measured with an avalanche photodiode (APD, Thorlabs APD110A2) connected to a 2.5 GHz digital oscilloscope. An infrared PMT (Hamamatsu H10330A-75) operated in photon counting mode detected the singlet oxygen phosphorescence. The spectral window of the PMT was limited to 1250–1350 nm by means of a band-pass filter. The pulses from the PMT were registered with a multichannel scaler (Stanford Res. Systems SR430). Results of ten consecutive measurements were recorded at all experimental conditions, taking the sum of 320 000 pulses in each measurement. This way the effect of photo-bleaching could be readily monitored throughout the experiment.

Absorption spectra of RuPhen in 0.9% NaCl isotonic solution were collected at different temperatures with a Varian CARY 500 Scan/UV-VIS-NIR spectrophotometer. The corresponding luminescence spectra were obtained by a Horiba Jobin-Yvon FluoroLog spectrophotometer at 447 nm excitation.

Data analysis

Typical evolution of the phosphorescence signals detected by the PMT around 1270 nm and the APD in the visible region is shown in Fig. 2. It can be seen that steady-state emission

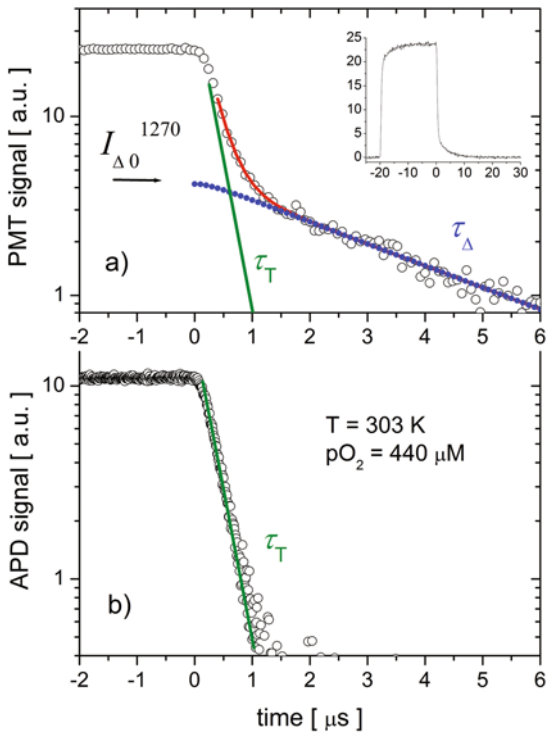

Fig. 2 Time-dependence of the emission intensities (logarithmic scale) at the end of the laser pulse and after switching the laser off at t = 0. (a) Experimental data (open circles) detected by the PMT around 1270 nm and fitted by eqn (6) – red curve. The contributions from singlet oxygen (dotted blue line) and RuPhen (solid green line) – as determined from the fitting procedure – are shown separately. The inset shows the PMT signal during the entire process (laser pulse and after switching the laser off) on a linear scale. (b) The APD signal in the visible spectral range fitted by a single exponential decay.

intensities are reached before the end of the 20 μs laser pulses. The time-scale zero-point (t = 0) is set at the end of the laser pulse in Fig. 2. After the laser is switched off, the APD signal starts to decay exponentially (Fig. 2b). This signal belongs to the decaying phosphorescence emission from the RuPhen ^{3}MLCT state. The intensity changes observed at 1270 nm (Fig. 2a) can be described by two components. First, there is a faster-decreasing signal originating from the infrared tail of the RuPhen phosphorescence spectrum. Second, a longer-lived component is observed, which belongs to singlet oxygen emission.

In the following we give a brief theoretical background for the analysis of the data acquired.

After switching the excitation beam off (at t = 0), the concentration of the RuPhen ^{3}MLCT state [T] decreases exponentially with a time constant τ_T:

$$\frac{1}{\tau_T} = k_0 + k_q[O_2]. \quad (1)$$

Here, k_0 is the quenching rate constant of the ^{3}MLCT state in the absence of oxygen, and k_q corresponds to the rate constant of ^{3}MLCT depopulation in reactions with ground state

molecular oxygen. The quenching rate constant k_0 can be further decomposed as[44]

$$k_0 = k_r + k_{nr} + k'\exp(-\Delta E/kT), \quad (2)$$

with k_r and k_{nr} being the rate constants of radiative and non-radiative deactivation, respectively. The third Arrhenius term in (2) stands for ^{3}MLCT transition to short-lived metal-centered d–d state of RuPhen, with a pre-exponential factor k' and an excitation energy of ΔE.[45]

Concentration changes $[\Delta]$ of $O_2(^1\Delta_g)$ after the laser pulse can be expressed as:

$$\frac{d[\Delta]}{dt} = k_q[O_2][T]f_\Delta^T - \frac{[\Delta]}{\tau_\Delta}. \quad (3)$$

The first term on the right side represents the production of $O_2(^1\Delta_g)$ by interaction of photo-excited RuPhen with molecular oxygen, f_Δ^T being the fraction of RuPhen ^{3}MLCT states quenched by oxygen yielding singlet oxygen. τ_Δ is the $O_2(^1\Delta_g)$ lifetime. Denoting the first term on the right side of (3) at initial time (t = 0) as $S_0 = k_q[O_2][T]_0 f_\Delta^T$, assuming steady-state concentrations $[\Delta]$ and $[T]$ at t = 0 and constant $[O_2]$ during the studied process, we obtain the solution of (3) as follows:

$$[\Delta] = \frac{S_0\tau_\Delta}{\tau_\Delta - \tau_T}\left(\tau_\Delta e^{-\frac{t}{\tau_\Delta}} - \tau_T e^{-\frac{t}{\tau_T}}\right). \quad (4)$$

The measured intensity decay at 1270 nm is a linear combination of phosphorescence contributions from $O_2(^1\Delta_g)$ and ^{3}MLCT:

$$I_{meas}^{1270} = c(k_\Delta^e[\Delta] + k_T^e[T]), \quad (5)$$

where k_Δ^e and k_T^e are the phosphorescence emission rate constants of $O_2(^1\Delta_g)$ and ^{3}MLCT, respectively, and c is an equipment specific proportionality factor. Substituting for $[\Delta]$ and $[T]$ into (5), the final fitting function for the measured infrared signal is obtained:

$$I_{meas}^{1270} = F_1\frac{\tau_\Delta}{\tau_\Delta - \tau_T}\left(\tau_\Delta e^{-\frac{t}{\tau_\Delta}} - \tau_T e^{-\frac{t}{\tau_T}}\right) + F_2 e^{-\frac{t}{\tau_T}}, \quad (6)$$

with four variable parameters: $F_1 = S_0 k_\Delta^e c$, $F_2 = [T]_0 k_T^e c$, τ_Δ and τ_T. It can be seen from Fig. 2a that the measured experimental data are well fitted with function (6). Assuming that the quenching of singlet oxygen by RuPhen is negligible (which is the case at low RuPhen concentration used in this work[39]), the precision of the fitting procedure can be improved using predefined τ_Δ values. This is especially true at low pO_2 levels with weak singlet oxygen signals. The temperature dependence of τ_Δ in water was reported by Jensen and co-authors[46] and there is an indication that τ_Δ is independent of the solution salinity.[47]

The $O_2(^1\Delta_g)$ phosphorescence contribution to the steady-state signal at t = 0, which can be determined from the fitted parameters, is proportional to the $O_2(^1\Delta_g)$ concentration at equilibrium $[\Delta]_0$:

$$I_{\Delta 0}^{1270} = F_1^{fit}\tau_\Delta = ck_\Delta^e[\Delta]_0. \quad (7)$$

$[\Delta]_0$ is also related to the quantum yield of $O_2(^1\Delta_g)$ production Φ_Δ as: $[\Delta]_0 = P_a\Phi_\Delta\tau_\Delta$, where P_a is the absorbed photon flux. It follows that Φ_Δ can be determined by comparing the measured F_1 values with those obtained for a reference molecule of known quantum yield Φ^{Ref}:

$$\Phi_\Delta = \Phi^{Ref}\frac{F_1}{F_1^{Ref}}\frac{\lambda_{las}^{Ref}}{\lambda_{las}}\frac{P_{las}^{Ref}}{P_{las}}, \quad (8)$$

where the product of the excitation laser power and wavelength, $P_{las}\cdot\lambda_{las}$, is proportional to the absorbed photon flux P_a. It is assumed here that the absorbances, the phosphorescence emission rate constants of singlet oxygen k_Δ^e and the equipment specific proportionality factor c are identical for the reference and measured samples. Rose Bengal dissolved in water was used in this work as a reference molecule with the corresponding quantum yield of the singlet oxygen production (at room temperature and air-saturated conditions) Φ^{Ref} = 0.76.[48]

Because of the relatively long switching time of the AOM (~400 ns), the PMT data acquired during the switching period do not obey function (6). Due to this fact, the very first 400 ns of the emission decay curves were not taken into account in the fitting procedure. The long switching time of the AOM also introduces an uncertainty into the timescale zero-point, which in principle may lead to erroneous evaluation of the extrapolated $O_2(^1\Delta_g)$ phosphorescence intensity at t = 0 (see (7) and Fig. 2a). Detailed analysis of the experimental curves showed that moving the timescale zero-point by 200 ns results in a ~5% difference in the fitted F_1 parameter, while the decay times τ_Δ and τ_T do not change. Regarding the quantum yield of singlet oxygen production as defined by (8), the error of F_1 is partially compensated by using the same fitting procedure (the same zero-point) for the reference sample.

The pO_2 dependence of Φ_Δ can be derived from the quantum yield of ^{3}MLCT state photo-excitation Φ_T as[32,39]

$$\Phi_\Delta = \Phi_T P_T^{O_2} f_\Delta^T, \quad (9)$$

where

$$P_T^{O_2} = \frac{k_q[O_2]}{k_0 + k_q[O_2]}. \quad (10)$$

According to previous investigations, Φ_T equals 1 for Ru(II) complexes.[32,39] $P_T^{O_2}$ stands for the fraction of ^{3}MLCT states quenched by interactions with oxygen. The values of k_0 and k_q can be obtained experimentally by fitting the pO_2 dependence of measured τ_T values with eqn (1). It follows that after the substitution of k_0 and k_q into (10) one can fit the measured pO_2 dependence of Φ_Δ with (9) using a single fitting parameter of f_Δ^T (the fraction of RuPhen ^{3}MLCT states quenched by oxygen yielding singlet oxygen).

Results and discussion

Absorption and emission spectra of air-saturated RuPhen solutions measured at different temperatures are shown in Fig. 3.

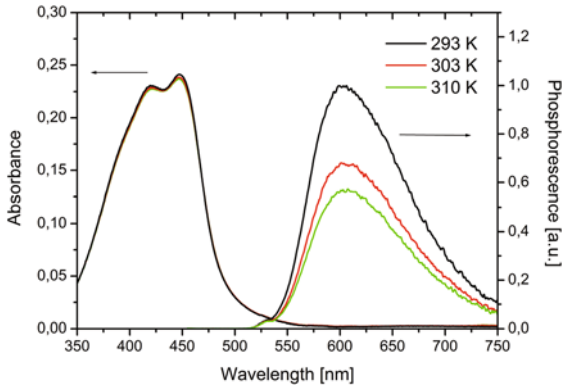

Fig. 3 Absorption and phosphorescence emission spectra of RuPhen dissolved in air-saturated 0.9% aqueous NaCl solution (pH = 6) measured at different temperatures. The RuPhen concentration was 33 μM and 1 μM in the case of absorption and emission measurements, respectively.

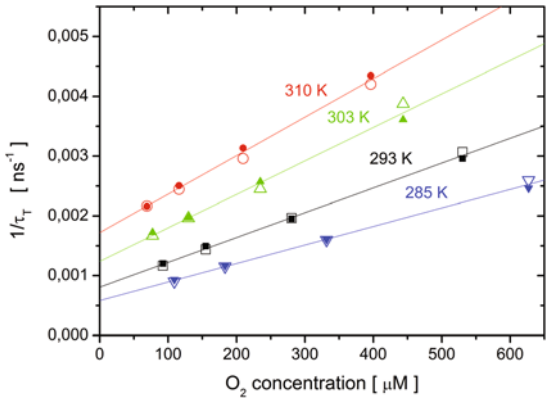

Fig. 4 Reciprocal values of RuPhen ^{3}MLCT lifetimes in 0.9% aqueous NaCl solution (pH = 6) measured at different temperatures and oxygen concentrations. Solid symbols: data evaluated from the decay of the APD signal (Fig. 2b) in the visible spectral domain. Open symbols: the ^{3}MLCT lifetime obtained by fitting the PMT signal measured around 1270 nm (Fig. 2a) with function (6). All the data are fitted with linear functions in accordance with (1).

It is observed that while the absorption is practically independent of temperature (in the studied temperature range), the phosphorescence signal decreases rapidly with an increase of temperature. Because of this fact, RuPhen can be also used as a temperature sensor, as it was shown by Köse and co-authors.[49]

Emission decay curves of RuPhen dissolved in 0.9% aqueous NaCl solution (pH = 6) were recorded in the temperature range of 285–310 K for different oxygen concentrations (not shown). The lifetime of the ^{3}MLCT state, τ_T, was evaluated first from the decay of the phosphorescence signal in the visible region detected by the APD (see Fig. 2b). It is noted that minor deviations from single exponential decay were observed in these data. The APD signal was better fitted by a two-exponential decay (not shown in Fig. 2b), where the second (longer-lived) component was possibly caused by a RuPhen photoproduct. As the intensity contribution of this component was typically below 1%, it was assumed that its effect on singlet oxygen production is negligible. The reciprocal values of the measured τ_T data are shown in Fig. 4 (solid symbols) as a function of pO_2.

The ^{3}MLCT lifetime was also obtained by fitting the emission intensity in the infrared region (PMT signal, Fig. 2a) by (6). The corresponding reciprocal τ_T values as a function of O_2 molar concentration are plotted in Fig. 4 with open symbols. There is a good match between the two data sets measured in the visible and infrared regions. The experimental data of Fig. 4 were fitted as linear functions of O_2 molar concentration. The obtained fitting parameters k_0 and k_q (see eqn (1)) are presented for various temperatures in Table 1. The standard errors of the fitted parameters are below 5% in all cases. To the best of our knowledge, the temperature dependence of k_q for RuPhen in water has not been reported yet. The experimental value of $k_q = 4.1 \times 10^9$ M^{-1} s^{-1} measured here at 293 K for RuPhen dissolved in 0.9% aqueous NaCl solution is in a good agreement with the room temperature data reported for RuPhen dissolved in water, $k_q = 4.05 \times 10^9$ M^{-1} s^{-1}.[32]

Table 1 The quenching rate constant of the ^{3}MLCT state in the absence of oxygen, k_0, and the rate constant of ^{3}MLCT depopulation in reactions with ground state oxygen, k_q, as determined by fitting the experimental data of Fig. 4 with (1)

Temperature [K]	k_0 [10^5 s^{-1}]	k_q [10^9 M^{-1} s^{-1}]
285	5.8	3.1
293	8.1	4.1
303	12.4	5.6
310	17.2	6.4

The quenching rate constant of the ^{3}MLCT state in the absence of oxygen, k_0, can be analyzed according to (2). The experimental k_0 values fitted with (2) are plotted as a function of $1/T$ in Fig. 5. For comparison, the results published for RuPhen dissolved in pure water (dashed line) and in sodium lauryl sulfate (NaLS) micellar solutions (dotted curve)[45] are also shown. From these data we can see that the presence of 0.9% NaCl in water changes the temperature dependence of k_0 as compared to RuPhen dissolved in pure water. Determination of k_0 was realized also in N_2-saturated aqueous RuPhen solution. The results (open circles in Fig. 5) are in good agreement with previous data of Dressick and co-authors (dashed line).[45] According to our present results, adding 0.9% NaCl to water leads to an increase of the excitation energy of the ^{3}MLCT→d–d transition of RuPhen from 40.5 to 49 kJ mol^{-1} (see the table inset in Fig. 5). At the same time, the sum of the de-excitation rate constants, $k_r + k_{nr}$, remains practically unchanged (about 3.2×10^5 s^{-1}). The higher ΔE in NaCl solution is close to the value reported for the NaLS micellar solution (ΔE = 50.5 kJ mol^{-1}).

The quantum yield of singlet oxygen production by RuPhen evaluated at different temperatures is plotted against O_2 molar concentration in Fig. 6. The experimental data were fitted by (9) using f_Δ^T as the only fitting parameter, while $P_T^{O_2}$ was deter-

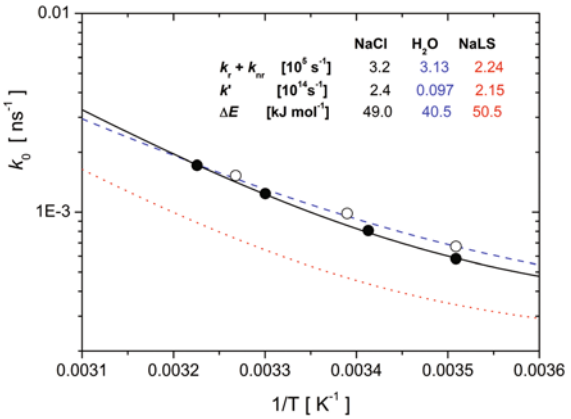

Fig. 5 The quenching rate constant (k_0) of the RuPhen ^{3}MLCT state in the absence of oxygen as a function of 1/T. Solid circles: present experimental data measured in 0.9% aqueous NaCl solution (as evaluated from the linear fits in Fig. 4). Solid line: fit to the experimental points according to (2). Open circles: present values measured in N_2-saturated water. Dashed and dotted lines are data published for RuPhen dissolved in water and in NaLS micellar solutions,[45] respectively. The parameters of $k_r + k_{nr}$, k' and ΔE (see (2)) are indicated in the inset.

mined from the obtained rate constants k_0 and k_q (see Table 1). The observed [O_2] dependence of singlet oxygen production by photo-excited RuPhen is well fitted by (9). The effect of temperature on the quantum yield of $O_2(^1\Delta_g)$ production is negligible. Within the experimental error the obtained values of f_Δ^T are identical (0.49 ± 0.03) in the entire studied temperature range (285–310 K).

As was mentioned in the Introduction section, the phototoxicity of RuPhen is still an open question. According to our present results, the quantum yield of singlet oxygen production under air-saturated conditions (and physiological temperatures, 310 K) is around 0.25. This value is not negligible, and thus singlet oxygen production has to be considered when thinking of the possible mechanisms of RuPhen phototoxicity.[30] On the other hand, our preliminary results obtained

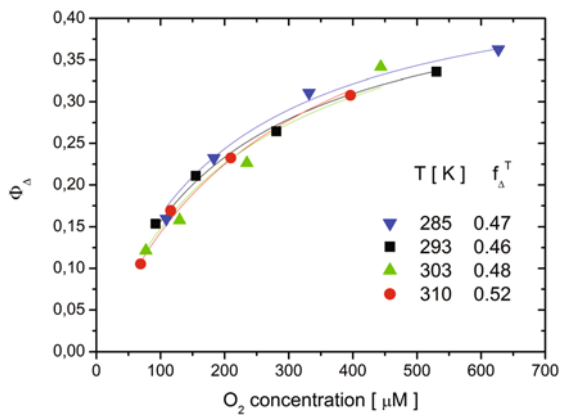

Fig. 6 The quantum yield of singlet oxygen production by RuPhen dissolved in 0.9% aqueous NaCl solution as a function of O_2 molar concentration. The experimental points were fitted by (9), the obtained values of f_Δ^T are shown in the inset.

with the CAM,[29] and the results of Dobrucki[28] and Asiedu *et al.*[27] indicate that under certain conditions (RuPhen concentrations below 1 mg kg^{-1} of body weight and light doses of less than 10 J cm^{-2} at 470 nm) the photo-toxicity of RuPhen is very low. Logically, the damage induced by photo-excited RuPhen will depend on the concentration used.[28] Importantly, the analysis of our results as well as the literature strongly suggest that, the tissular and intra-cellular localization play a key role on the potency of RuPhen. Further experiments are needed to find feasible conditions for the application of RuPhen as an *in vivo* pO_2 sensor, including the development of optimized derivations and formulations. These are beyond the scope of this work, however.

Conclusions

The quantum yield of singlet oxygen production by photo-excited RuPhen (dissolved in 0.9% aqueous NaCl solutions) and the depopulation rates of the RuPhen ^{3}MLCT state have been measured at different temperatures and oxygenation conditions. The quasi-continuous excitation scheme was successfully tested for the suppression of RuPhen photo-bleaching. It was shown that RuPhen is able to generate singlet oxygen with significant quantum yield in a broad temperature range, which needs to be taken into account when using RuPhen for *in vivo* pO_2 measurements.

Acknowledgements

The authors would like to thank Dr Erik Sedlák for the possibility to realize temperature dependent UV-VIS measurements at the Department of Biochemistry, P.J. Safarik University in Kosice. We also gratefully acknowledge editorial assistance by Matthieu Zellweger from ISIC-LCOM at EPFL in Lausanne. This work was supported by SCIEX-MNSch (Project Codes 13.029 and 10.142), the grants of the Slovak Ministry of Education VEGA 1/1246/12, APVV-0242-11, the FP7 EU CELIM 316310 project and the project no. 205320_147141 of the Swiss National Science Foundation. This work was also supported by the projects SEPO-II (26220120039) and NanoBioSens (26220220107) of the Operation Programme Research and Development funded by the European Regional Development Fund.

Notes and references

1 B. C. Wilson and M. S. Patterson, *Phys. Med. Biol.*, 2008, **53**, R61–R109.
2 A. P. Castano, P. Mroz and M. R. Hamblin, *Nat. Rev. Cancer*, 2006, **6**, 535–545.
3 C. A. Robertson, D. H. Evans and H. Abraharnse, *J. Photochem. Photobiol., B*, 2009, **96**, 1–8.
4 R. P. Mason, D. Zhao, J. Pacheco-Torres, W. Cui, V. D. Kodibagkar, P. K. Gulaka, G. Hao, P. Thorpe,

E. V. Hahn and P. Peschke, *Q. J. Nucl. Med. Mol. Imaging*, 2010, **54**, 259–280.
5 M. R. Horsman, *Int. J. Radiat. Oncol., Biol., Phys.*, 1998, **42**, 701–704.
6 F. Piffaretti, A. M. Novello, R. S. Kumar, E. Forte, C. Paulou, P. Nowak-Sliwinska, H. van den Bergh and G. Wagnieres, *J. Biomed. Opt.*, 2012, **17**, 115007.
7 J. H. Woodhams, A. J. MacRobert and S. G. Bown, *Photochem. Photobiol. Sci.*, 2007, **6**, 1246–1256.
8 J. P. T. Ward, *Bba-Bioenerg.*, 2008, **1777**, 1–14.
9 S. Lahiri, A. Roy, S. M. Baby, T. Hoshi, G. L. Semenza and N. R. Prabhakar, *Prog. Biophys. Mol. Biol.*, 2006, **91**, 249–286.
10 D. B. Papkovsky and R. I. Dmitriev, *Chem. Soc. Rev.*, 2013, **42**, 8700–8732.
11 R. I. Dmitriev and D. B. Papkovsky, *Cell. Mol. Life Sci.*, 2012, **69**, 2025–2039.
12 H. J. C. M. Sterenborg, J. W. de Wolf, M. Koning, B. Kruijt, A. van den Heuvel and D. J. Robinson, *Opt. Express*, 2004, **12**, 1873–1878.
13 J. M. Vanderkooi, G. Maniara, T. J. Green and D. F. Wilson, *J. Biol. Chem.*, 1987, **262**, 5476–5482.
14 D. F. Wilson, W. M. F. Lee, S. Makonnen, O. Finikova, S. Apreleva and S. A. Vinogradov, *J. Appl. Physiol.*, 2006, **101**, 1648–1656.
15 T. K. Stepinac, S. K. Chamot, E. Rungger-Brandle, P. Ferrez, J. L. Munoz, H. van den Bergh, C. E. Riva, C. J. Pournaras and G. A. Wagnieres, *Invest. Ophthalmol. Visual Sci.*, 2005, **46**, 956–966.
16 J. N. Demas and B. A. Degraff, *Makromol. Chem., Macromol. Symp.*, 1992, **59**, 35–51.
17 W. Y. Xu, R. C. Mcdonough, B. Langsdorf, J. N. Demas and B. A. Degraff, *Anal. Chem.*, 1994, **66**, 4133–4141.
18 J. N. Demas, D. Diemente and E. W. Harris, *J. Am. Chem. Soc.*, 1973, **95**, 2.
19 J. N. Demas and G. A. Crosby, *J. Mol. Spectrosc.*, 1968, **26**, 72–77.
20 H. Kobayashi and Y. Kaizu, *Coord. Chem. Rev.*, 1985, **64**, 53–64.
21 Z. Rosenzweig and R. Kopelman, *Sens. Actuators, B*, 1996, **36**, 475–483.
22 E. R. Carraway, J. N. Demas, B. A. Degraff and J. R. Bacon, *Anal. Chem.*, 1991, **63**, 337–342.
23 J. H. Koch, W. P. Rogers, F. P. Dwyer and E. C. Gyarfas, *Aust. J. Biol. Sci.*, 1957, **10**, 342–350.
24 A. Yadav, T. Janaratne, A. Krishnan, S. S. Singhal, S. Yadav, A. S. Dayoub, D. L. Hawkins, S. Awasthi and F. M. MacDonnell, *Mol. Cancer Ther.*, 2013, **12**, 643–653.
25 M. Paxian, S. A. Keller, B. Cross, T. T. Huynh and M. G. Clemens, *Am. J. Physiol.: Gastrointest. Liver Physiol.*, 2004, **286**, G37–G44.
26 T. N. Tan, R. H. Weston and J. P. Hogan, *Int. J. Appl. Radiat. Isot.*, 1971, **22**, 301–308.
27 J. K. Asiedu, J. Ji, M. Nguyen, N. Rosenzweig and Z. Rosenzweig, *J. Biomed. Opt.*, 2001, **6**, 116–121.
28 J. W. Dobrucki, *J. Photochem. Photobiol., B*, 2001, **65**, 136–144.
29 V. Huntosova, S. Gay, P. Nowak-Sliwinska, S. K. Rajendran, M. Zellweger, H. van den Bergh and G. Wagnieres, *J. Biomed. Opt.*, 2014, **19**, 77004.
30 M. Zarebski, M. Kordon and J. W. Dobrucki, *Photochem. Photobiol.*, 2014, **90**, 709–715.
31 D. Garcia-Fresnadillo, Y. Georgiadou, G. Orellana, A. M. Braun and E. Oliveros, *Helv. Chim. Acta*, 1996, **79**, 1222–1238.
32 A. A. Abdel-Shafi, M. D. Ward and R. Schmidt, *Dalton Trans.*, 2007, 2517–2527.
33 S. A. Poteet, M. B. Majewski, Z. S. Breitbach, C. A. Griffith, S. Singh, D. W. Armstrong, M. O. Wolf and F. M. MacDonnell, *J. Am. Chem. Soc.*, 2013, **135**, 2419–2422.
34 Y. J. Liu, C. H. Zeng, J. H. Yao, F. H. Wu, L. X. He and H. L. Huang, *Chem. Biodiversity*, 2010, **7**, 1770–1783.
35 F. Gao, H. Chao, Y. F. Wei, Y. X. Yuan, B. Peng, X. Chen, K. C. Zheng and L. N. Ji, *Helv. Chim. Acta*, 2008, **91**, 395–410.
36 M. Atsumi, L. Gonzalez and C. Daniel, *J. Photochem. Photobiol., A*, 2007, **190**, 310–320.
37 P. R. Ogilby, *Chem. Soc. Rev.*, 2010, **39**, 3181–3209.
38 P. R. Ogilby, *Photochem. Photobiol. Sci.*, 2010, **9**, 1543–1560.
39 A. A. Abdel-Shafi, D. R. Worrall and A. Y. Ershov, *Dalton Trans.*, 2004, 30–36.
40 R. Schmidt, *J. Phys. Chem. A*, 2006, **110**, 2622–2628.
41 S. Lee, L. Y. Zhu, A. M. Minhaj, M. F. Hinds, D. H. Vu, D. I. Rosen, S. J. Davis and T. Hasan, *J. Biomed. Opt.*, 2008, **13**, 034010.
42 S. Lee, D. H. Vu, M. F. Hinds, S. J. Davis, A. Liang and T. Hasan, *J. Biomed. Opt.*, 2008, **13**, 064035.
43 B. B. Benson and J. D. Krause, *Limnol. Oceanogr.*, 1984, **29**, 620–632.
44 J. N. Demas and B. A. Degraff, *Anal. Chem.*, 1991, **63**, A829–A837.
45 W. J. Dressick, J. Cline, J. N. Demas and B. A. Degraff, *J. Am. Chem. Soc.*, 1986, **108**, 7567–7574.
46 R. L. Jensen, J. Arnbjerg and P. R. Ogilby, *J. Am. Chem. Soc.*, 2010, **132**, 8098–8105.
47 L. P. F. Aggarwal, M. S. Baptista and L. E. Borissevitch, *J. Photochem. Photobiol., A*, 2007, **186**, 187–193.
48 F. Wilkinson, W. P. Helman and A. B. Ross, *J. Phys. Chem. Ref. Data*, 1993, **22**, 113–262.
49 M. E. Köse, B. F. Carroll and K. S. Schanze, *Langmuir*, 2005, **21**, 9121–9129.